Untying the Bundles of Solution-Synthesized Graphene Nanoribbons for Highly Capacitive Micro-Supercapacitors

Zhaoyang Liu, Yunbin Hu, Wenhao Zheng, Can Wang, Walid Baaziz, Fanny Richard, Ovidiu Ersen, Mischa Bonn, Hai I. Wang, Akimitsu Narita, et al.

Untying the Bundles of Solution Synthesized Graphene Nanoribbons for Highly Capacitive Micro-Supercapacitors

*Zhaoyang Liu, Yunbin Hu, Wenhao Zheng, Can Wang, Walid Baaziz, Fanny Richard, Ovidiu Ersen, Mischa Bonn, Hai I. Wang, Akimitsu Narita, Artur Ciesielski, Klaus Müllen, Paolo Samorì**

Dr. Z. Liu, Dr. C. Wang, Dr. F. Richard, Dr. A. Ciesielski, Prof. Dr. P. Samorì
Université de Strasbourg and CNRS, ISIS, 8 allée Gaspard Monge, 67000 Strasbourg, France
*Corresponding author: samori@unistra.fr

Dr. Y. Hu, W. Zheng, Prof. Dr. M. Bonn, Dr. H. I. Wang, Dr. A. Narita, Prof. Dr. K. Müllen
Max Planck Institute for Polymer Research, Ackermannweg 10, 55128 Mainz, Germany

Dr. Y. Hu
College of Chemistry and Chemical Engineering, Central South University, Changsha, Hunan 410083, P. R. China

Dr. W. Baaziz, Prof. Dr. O. Ersen
Institut de Physique et Chimie des Matériaux de Strasbourg (IPCMS), UMR 7504 Université de Strasbourg and CNRS, 23 rue du Loess, 67034 Strasbourg, France

Prof. Dr. A. Narita
Organic and Carbon Nanomaterials Unit, Okinawa Institute of Science and Technology Graduate University, 1919-1 Tancha, Onna-son, Kunigami, Okinawa 904-0495, Japan

Keywords: graphene nanoribbon, bundles, shear-mix exfoliation, molecular amphiphilicity , micro-supercapacitor

Abstract

The precise bottom-up synthesis of graphene nanoribbons (GNRs) with controlled width and edge structures may compensate graphene's limitations, such as the absence of an electronic bandgap. On the same time, GNRs maintain graphene's unique lattice structure in one dimension and provide more open edge structures compared to graphene, thus allowing faster ion diffusions, which are highly promising for energy storage systems. However, the current solution synthesized graphene nanoribbons suffer from severe aggregation due to the strong π-π interactions, which limits their potential applications. Thus, it is indispensable to develop a facile and scalable approach to exfoliate the GNRs from the post-synthetic aggregates yielding individual nanoribbons. Here, we demonstrate a high-shear mixing approach to untie the GNR bundles into practically individual GNRs, by introducing suitable molecular interactions. The micro-supercapacitors (MSCs) electrode based on solution-processed GNR film exhibits an excellent volumetric capacitance of 355 F cm^{-3} and a high power density of 550 W cm^{-3}, reaching the state-of-the-art performance of graphene and related carbon materials, and thus demonstrating the great potential of GNRs as electrode materials for future energy storage.

1. Introduction

Graphene nanoribbons (GNRs) are narrow strips of graphene with widths below 10 nm that have recently emerged as a novel class of 1D nanocarbon materials. GNRs exhibit tunable molecular structures and thus unique properties, among others including adjustable electronic and optical properties, spin-polarized edge states, superlubricity, and feasible integrations for molecular heterojunctions.[1] Notably, due to the quantum confinement effect, GNRs' 1D structure is accompanied by the opening of an electronic band gap compared to the 2D graphene. This paves the way to digital-logic devices operating at room temperature, while maintaining high charge carrier mobilities.[2] Consequently, GNRs are superior building blocks for future nanoscale electronics/optoelectronics, spintronics, as well as energy storage systems.[3] In particular, the presence of abundant open edges in GNRs makes them suitable candidates for high-performance micro-supercapacitors (MSCs). This is because the magnitude of the normalized capacitance of graphene-based electrode materials has been reported to increase with the incrasing amount of carbon atoms placed in open edge structures.[4]

Similarly to the fabrication of 2D materials, there are two main approaches that can be employed for the production of GNRs, i.e., top-down and bottom-up. The top-down approach includes E-beam lithography (EBL) patterning of graphene,[5] liquid-phase chemical derivatization of graphene,[3f] or unzipping of carbon nanotubes.[6] However, cutting graphene with atomic precision into GNRs with well-defined width and edge structures is out of reach for these techniques. Furthermore, the presence of defective edges gives rise to scattering and localization of electrons, which are detrimental to the electronic properties.[7] On the contrary, through the alternative bottom-up synthetic approaches, both the geometric and electronic characteristics of GNRs can be well-tuned through the design and synthesis of ad-hoc molecular precursors, by taking advantage of the toolbox of organic synthesis methods.[8] The synthesis of GNRs can be achieved through solution processes based on conventional organic chemistry or surface-assisted fabrication combining modern physics methods.[9] The surface-assisted

synthesis usually requires ultrahigh vacuum conditions during the growth, providing limited amounts of GNR samples, where a subsequent film transfer process is also required in order to remove the catalytic substrates before further applications. Alternatively, the solution-phase synthesis holds potential for large-scale fabrication of solution-processable GNRs.[10] However, besides the challenges in structural perfection and functionalization during the sophisticated chemical synthesis of GNRs, the decreasing solubility of larger and longer GNRs in organic solvents are limiting their application potential.[8, 11] Due to the strong π-π stacking interactions between adjacent ribbons, synthesized GNRs unavoidably have a strong tendency to form aggregated bundles in solution phases similar to carbon nanotubes, hampering the possibility of isolating the monodisperse nanoribbons.[3a, 12] To date, efficient and scalable approaches have not been properly addressed for the exfoliation of such GNRs. Therefore, the optimization of the solution synthesized GNRs processing is essential to take full advantage of the unique characteristics of GNRs, thus effectively enlarge the catalogue of materials for current carbon-based nanoscience.

Herein, we exploit non-covalent interactions between GNRs and ad-hoc small organic molecules and make use of the high-shear mixing approach to exfoliate GNR bundles into individual species. The use of alkyl chain substitution at the edges of GNRs has become a successful approach towards significant improvement of the GNR solubility, yet the addition of sp^3 carbons drastically dilute the electronic properties of the GNRs and assemblies thereof. Thus, we apply thermal annealing treatment to remove the alkyl chains, thereby significantly improving the overall electrical transport properties of the obtained GNR films, being beneficial for their applications in MSCs. The MSC electrode based on solution-processed GNR film exhibits an excellent volumetric capacitance of 355 F cm^{-3} and a high power density of 550 W cm^{-3}, comparable to state-of-the-art performance based on graphene-related materials, thus demonstrating the great potential of finely dispersed GNRs produced in large-scale as promising materials for future energy storage.

2. Results and Discussion

Figure 1a and Figure S1a shows the molecular structure of the employed alkyl substituted GNR with the "cove"-type (or also called gulf) edges and the width of four carbon atoms at the narrowest, i.e., 4-CGNR, with lengths exceeding 200 nm, as synthesized following previously reported procedures.[10] These 4-CGNRs typically exhibit an aggregated bundle-like structure (several 4-CGNRs tightly packed together, as portrayed in Figure 1b) with individual GNR aggregating via strong π-π interactions, withstanding even prolonged sonication treatment. [10, 12b, 12d, 12h] Since high-shear mixing treatment of graphite is capable of breaking the van de Waals interactions between the 2D sheets to produce high-quality graphene in large quantities,[13] we propose to extend this approach to untie the bundles of 4-CGNRs. Figure 1c schematically illustrates the high-shear mixing process for the exfoliation of 4-CGNRs bundles, with the ultrafast rotation of rotor blades generating a powerful enough suction that leads the bundles at the bottom into the working head followed by extrusion through the perforations with intense hydraulic shear. *N*-methyl-2-pyrrolidone (NMP) is chosen as the operating solvent due to its matching surface energy with that of the graphene lattice and it is known as a good solvent for graphene and carbon nanotube exfoliation.[13-14] With 4500 rpm rotor speed, the 4-CGNRs bundles can be readily exfoliated within 20 mins. The electronic absorption of GNRs is very sensitive to their aggregation states. The UV-Vis spectrum is thus employed to quantitatively examine the exfoliation process.[15] The UV-Vis absorption spectra of as-exfoliated 4-CGNR dispersions (Figure 1d, from 0.001 to 0.1 mg mL^{-1} in NMP) are dominated by an optical transition at ~570 nm due to excitonic transition, which agrees well with previous theoretical findings.[16] Figure 1e further displays the absorbance values at 570 nm as a function of the concentration, which complies with the Beer-Lambert behavior at lower concentrations with a good linear fitting (R^2=0.996), suggesting good homogeneity of the achieved dispersion and thus the successful exfoliation of the 4-CGNR bundles. Such a phenomenon also

demonstrates a decreased content of the 4-CGNRs' aggregated states in diluted conditions, guiding the direction for further optimization of the employed shear mixing process. The Raman spectrum of the 4-CGNR after deposition to form a dry film (measured under 532 nm laser with 0.03 mW power, Figure 1f) exhibits the typical first-order D, G, and second-order 2D, D+D', 2D' peaks, confirming the undisrupted graphenic nature of GNRs after shear mixing exfoliation. More importantly, the observed width-specific radial breathing-like mode (RBLM) peak located at 233 cm^{-1} provides evidence for the molecular structure of exfoliated 4-CGNRs (inset in Figure 1f) as well as illustrates the high uniformity of precisely defined lateral width (~1 nm) of the 4-CGNRs composing the film.[1a, 10, 17] Figure 1g illustrates the potential scale-up production of finely dispersed 4-CGNRs by such shear mixing, with 1 liter produced within 1 hour at current lab scale. We believe that this can be easily upgraded to massive industrial production speed with tens of L/h. The obtained dispersion exhibits a shelf life exceeding one month without significant precipitation, which might be attributed to the matching surface energies between the NMP solvent and the basal plane of 4-CGNRs (same as graphene). In contrast, the exfoliation in tetrahydrofuran (THF) works initially, yet it results in quick precipitation after 1 day (Figure S1). In addition, the 4-CGNRs dispersion in NMP can also be obtained *via* prolonged ultrasonication (1 hour). However, the use of NMP as an exfoliation medium only yields in a very broad peak of the absorption curve (Figure S1), which suggests the presence of various aggregation states within the obtained dispersion. Therefore, the employed shear-mixing protocol is more efficient than the conventional sonication method, in regard to quality and scalability of the obtained GNR dispersion.

To further optimize the shear mixing conditions, 8000 rpm rotor speed was applied and found to yield an absorption curve similar to the one obtained when exploiting 4500 rpm (**Figure 2a**). Since the improvement in the GNR exfoliation upon elevating rotor speed is still limited, ad hoc molecular approaches should be considered. The decoration of GNRs edges with alkyl side chains is aimed at improving their solubility, but their presence may also hinder

the interactions between the core of GNRs and the solvent molecules during the shear mixing. Thus, for better untying the bundles of GNRs, competitive non-covalent interactions between the GNR and a suitably designed small molecule can be employed. Ideally, such a molecule should have a high affinity for both the GNR core and the alkyl side chains with the goal of 'dragging' the individual 4-CGNRs out of the bundles during shear mixing exfoliation. The chosen additive molecules should feature a strong affinity for both 4-CGNRs and to NMP molecules, which can also act as dispersion-stabilizing agents after the exfoliation.[18] In this regard, docosanoic acid (DA, whose molecular structure is shown in the inset of Figure 2a) exposing a highly polar -COOH group has been employed to promote intermolecular non-covalent interactions with 4-CGNRs during the exfoliation process. In particular, the linear alkanes can be foreseen to interact with the alky chains at the edges of 4-CGNRs and the terminating -COOH groups strongly interact with the polar NMP molecules, marking the importance of the amphiphilicity of the additive molecules. Upon exfoliation with the same rotor speed, as expected, the peak in the absorption spectra of 4-CGNR in NMP becomes significantly sharpened after the introduction of DA molecules. Previous studies evidenced the partial overlapping of 4-CGNR dispersion absorption between experimental (GNRs prepared via ultrasonication) and theoretical results, whereas the ratio between the absorbance at 470 nm and 570 nm (Abs_{470nm}/Abs_{570nm}) can be extracted as 33% from theoretical calculations and 71% from the experimental results.[19] To our surprise, the shear-mixing approach yields only 48% for Abs_{470nm}/Abs_{570nm} from the absorption curve with full width at half maximum (FWHM) of 154 nm, which is mostly overlapping with the one from ab-initio density functional theory (DFT) calculations (FWHM of ~130 nm), demonstrating the great potential of such shear mixing exfoliation of GNRs with high-quality dispersion.[19-20] To better illustrate the importance of such molecular amphiphilicity, 1-phenyloctane (with 20 wt.% content of 4-CGNRs) is also employed as a reference additive molecule to non-covalently stabilize individual 4-CGNRs during the exfoliation process as a control experiment. While the linear

alkanes are expected to interact with the alky chains at the edges of 4-CGNRs, the terminating low polar phenyl groups can also interact with the NMP molecules, although in a much weaker way. In line with our expectation, the absorption peak of the as-prepared dispersion is broader than the case of DA, suggesting more aggregates. This result highlights the key importance of additive molecule's amphiphilicity during the shear-mixing process. Moreover, further filtration (200 nm pore size of the PTFE membrane) does not significantly sharpen the absorption peak, indicating the high homogeneity of the obtained 4-CGNR dispersion (Figure S2). An optical bandgap of ~1.9 eV is also revealed, which is consistent with the previous reports.[10] The high-resolution transmission electron microscopy (HR-TEM) reveals individual 4-CGNRs (Figure 2b). Atomic force microscope (AFM) further portrays the narrow strip-like structures of well-exfoliated 4-CGNRs on a highly oriented pyrolytic graphite (HOPG) surface (Figure 2c and d). The height profile shows the majority of the 4-CGNRs' thickness lies in the range of 0.3-0.4 nm (Figure S3), which corresponds to the planar structure of 4-CGNR with one carbon atom thickness. Such a face-on orientation of the 4-CGNR onto the HOPG basal plane is in good agreement with previous observations on large polycyclic aromatic hydrocarbons physisorbing in monomolecular thick films on the same substrate. The strong interaction between HOPG and 4-CGNR could further assist the disaggregation of bundles to promote physorption of monolayer thick ribbons.[21] Moreover, the dominating lateral size of 4-CGNR is around 200 nm (over 50%). In Figure 2d, the phase image demonstrates the high homogeneity of the 4-CGNRs, with high contrast with respect to the HOPG substrate. This high-shear mixing approach is highly promising to overcome the commonly existing limitations in the solubility of bottom-up synthesized GNRs with various width and edge structures, which is of utmost importance for their potential applications.

The introduction of long alkyl chains in the GNRs' structures typically improves their low solubility in organic solvents, yet their presence generally limits the electrical transport properties of GNR films. Here, we employ a vacuum annealing process to thermally remove

the alkyl chains from the periphery of 4-CGNR. The film of 4-CGNR is heated at 400 °C in high vacuum (~10^{-7} mbar) for 10 hours. X-ray photoelectron spectroscopy (XPS) is employed to determine the ratio between sp^2 and sp^3 carbon of the 4-CGNR, before and after annealing process. As illustrated in **Figure 3a** and b, the self-fitted C 1s high resolution spectrum reveals that the ratio between sp^2 carbon (284.5 eV) and sp^3 carbon (285.5 eV) enhances significantly from 4.3 to 20 after annealing, providing unambiguous evidence for the (at least partial) removal of the alkyl chains. The Raman spectra recorded before and after annealing provide a similar output (Figure S4), suggesting that the annealing employed towards the removal of the alkyl chains at the edges does not introduce defects into the basal planes of GNRs. The electronic properties of 4-CGNR film are assessed before and after the annealing process by integrating the nanostructures in a bottom-contact field-effect transistor (FET) with back gate. The output characteristic at V_g=0 V reveals that the thermal annealing of the same 4-CGNR FET device determines a ~3 orders of magnitude increase in the measured source-drain current (I_{ds}) values, providing strinking evidence of the greatly improved electrical conductivity of the GNR films after removal of the alkyl chains (Figure S5). To provide insights into the origin of the enhanced electrical transport properties, we employ optical-pump terahertz (THz)-probe spectroscopy to evaluate the charge carrier transport properties of 4-CGNR films before and after annealing treatment. THz spectroscopy is a well-established contact-free, ultrafast technique, which allows us to investigate intra-GNR carrier transport [22]. Figure 3c shows the time-resolved photoconductivity for 4-CGNR film before and after annealing treatment, following optical excitation by 3.10 eV laser pulses. The sub-picosecond rise of the real conductivity implies the photogeneration of free carrier, followed by a rapid decay which could be attributed to the formation of bounded electron-hole pairs.[22b, 23] Significantly, we find negligible difference in both conductivity amplitude and dynamics for 4-CGNRs before and after annealing treatments, suggesting the electrical properties of the individual 4-CGNRs remain unchanged after removal of the alkyl chains[22b]. Further studies on the frequency-

resolved conductivity, as shown in Figure 3d, demonstrate identical conductivity amplitude and dispersion, which confirms again that the annealing treatment does not affect the charge transport properties of individual GNRs while removing the alkyl chains. Based on this result, we can attribute the improved electrical conductivity of GNR films observed in FET devices to the enhanced inter-GNR transport, as a direct consequence of the alkyl chain removal upon annealing.

Upon removal of the alkyl chains at their edges, the significantly improved electronic conductivity within the films combined with the exposed open edge structures, render the 4-CGNRs promising electrode materials for MSCs.[24] To evaluate the electrochemical performance of 4-CGNR, we fabricated solid-state MSCs based on the 4-CGNR films. Briefly, the 4-CGNR film was obtained via a vacuum filtration-assisted "dry transfer" method.[25] The 4-CGNR dispersion was first filtered through a PTFE membrane to obtain a "filtered cake", which was subsequently pressed against the precleaned SiO_2/Si substrate with constant pressure for 3 hours. The 4-CGNR film was thus transferred onto the SiO_2/Si substrate, followed by a thermal annealing process at 400 °C in high vacuum. Well-established lithography techniques were employed to produce 4-CGNR based interdigitated microelectrodes for MSCs.[24-25] The gold current collectors were deposited on top of the 4-CGNR film (~100 nm) through a homemade shadow mask. The uncovered part of the 4-CGNR film was etched away by oxygen plasma, and a polymer gel electrolyte H_2SO_4/polyvinyl alcohol (H_2SO_4/PVA) was drop-cast onto the interdigitated microelectrodes with overnight solidification. Thus, the solid-state MSCs based on 4-CGNR microelectrodes with an in-plane device geometry were achieved. To evaluate the electrochemical performance of the as-fabricated MSCs, cyclic voltammetry (CV) was performed at different scan rates ranging from 10 to 10000 mV s^{-1}, with a potential window from 0 to 1 V (**Figure 4** and Figure S6). The MSCs based on 4-CGNR microelectrodes all exhibit a typical nearly rectangular shape in the CV curve, even at a high operating speed of 10 V s^{-1}. This demonstrates the pronounced capacitive performance based on electric double-layer

capacitance, as inherited from their graphene structure with preserved excellent electronic properties. The distorted shape of the CV curves in Figure 4 is mainly because of the resistance of MSC, which is due to the still limited electrical conductivity of 4-CGNR compared with top-down achieved graphene materials. Noteworthy, such MSCs can be operated at a maximum speed of 100 V s^{-1}, which is two orders of magnitude higher than that of conventional sandwiched-structured supercapacitors, displaying its ultrafast charging/discharging capability.[26] Remarkably, the 4-CGNR microelectrodes deliver a maximum areal capacitance of 3.6 mF cm^{-2} and a volumetric capacitance (C_{vol}) of 355 F cm^{-3} at the scan rate of 10 mV s^{-1}, both of which outperform most *state-of-the-art* MSCs based on graphene or other nanocarbon materials, i.e., 0.2-2 mF cm^{-2} and 0.76-71.6 F cm^{-3}.[26-27] Moreover, the achieved C_{vol} is highly comparable to the best performances reported so far, e.g. 307 F cm^{-3} based on armchair type GNRs produced via chemical vapor deposition,[24] 359 F cm^{-3} based on electrophoretic deposited RGO,[28] 376 F cm^{-3} based on high-temperature annealed (1000 °C) of graphene hydrogel,[29] 410 F cm^{-3} based on carbide-derived carbon,[30] ~500 F cm^{-3} based on nitrogen-doped mesoporous carbon,[31] as well as 582 F cm^{-3} based on sulfur-doped graphene.[32] Such superior capacitive performances might be attributed to the synergetic effect of much shortened ion diffusion pathways from the in-plane device geometry, enhanced electrical transport for the films, and the vastly introduced open edge structures of 4-CGNRs with excellent electronic properties. The mass loading of the 4-CGNR film for the micro-supercapacitor is around 1.2 g/cm3, which suggests a highly compact structure and can be partially attributed to the employed filtration-assisted dry transfer methods. The high mass loading of the 4-CGNR film is one of the essential reasons for the obtained excellent volumetric capacitance.

Figure 5a shows the evolution of C_{vol} for various scan rates, which demonstrates the excellent rate capability of the 4-CGNR as electrode material in MSCs. As compared with the maximum C_{vol} of 355 F cm^{-3} at 0.01 V/s, the capacitance retention is remarkably high as 45% when operating speed increase to 3 orders of magnitudes higher (10 V/s), and 20% retention as

operating speed increase to 4 orders of magnitudes higher (100 V/s). Moreover, Figure 5b displays a nearly linear correlation between the logarithmic discharge current values and the applied scan rates. These results indicate that the 4-CGNR based MSC is capable of undergoing an ultrafast charging/discharging process while maintaining outstanding capacitance, which can be further translated into high instantaneous power. Electrochemical impedance spectroscopy (EIS) of 4-CGNR MSC is performed from 0.01 Hz to 100 kHz (Figure S7). The MSC in a high-frequency Nyquist plot shows a low equivalent series resistance (ESR) of 12 Ω. No semicircle is observed, which suggests ultrasmall charge transfer resistance (CTR). The phase angle plot against frequency reveals the characteristic frequency f_0 at the phase angle of -45° is 1654 Hz, which corresponds to a time constant τ_0 ($\tau_0 = 1/f_0$, the minimum time required to discharge ≥ 50% of all the energy from the MSC) of only 0.6 ms. Therefore, the features of low ESR, ultrasmall CTR, and short τ_0 validate the excellent charging/discharging capability of 4-CGNR MSC and demonstrates the potential high-power density of the micro-device. Remarkably, the 4-CGNR MSC delivers a power density of 550 W cm^{-3}. The Ragone plot lists the volumetric performance of 4-CGNR based MSC and some current market-dominating energy storage systems (Figure 5c), which illustrates that the power density of 4-CGNR based MSC, is about 1 order of magnitude higher than that of typical aluminum electrolytic capacitors (3V/300 μF), and several orders of magnitude higher than that of conventional sandwich-structured supercapacitors based on graphene as well as the commercial cell (3.5 V/25 mF).[26, 33] Furthermore, the MSC exhibits an energy density of 8 mWh cm^{-3}, which also outperforms the conventional capacitors/supercapacitors and is comparable to that of commercially available lithium thin-film battery (4V/500 μAh, 10 mWh cm^{-3}).[26, 32] Meanwhile, the long-term cycling stability of the MSC is tested for 10000 cycles at a high operating speed of 1 V/s, which displays high capacitance retention up to 93%, thus demonstrating the potential of the 4-CGNR based MSC (Figure 5d).

3. Conclusion

In conclusion, we have developed a facile high-shear mixing approach to untie the bundles of GNRs into a well-separated GNR form, by introducing additive molecules with amphiphilicity towards both GNR and solvent molecules. The achieved GNR dispersion has an almost overlapping absorption curve as compared with the one resulting from DFT calculations. The employed shear mixing approach can scale-up the production of solution-processed GNRs for energy storage systems. MSCs are fabricated based on 4-CGNR microelectrodes, which feature promising electrochemical performance, i.e., high operating speeds and volumetric capacitance, excellent power and energy densities outperforming state-of-the-art MSCs based on graphene or other nanocarbon materials, and highly comparable to commercially available thin-film batteries and capacitors. Future optimization of the GNR synthesis with improved design concepts, e.g., more suitable molecular precursors with improved solubility and stable zig-zag edge structures for ultra-long and metallic GNR growth with fewer defects and higher solubility, may pave the way for such unique 1D nanocarbon material as a candidate for ultrathin and wearable electronics.

Supporting Information

Supporting Information is available from the Wiley Online Library or from the author.

Acknowledgements

We acknowledge funding from the European Commission through the ERC project SUPRA2DMAT (GA-833707) and the Graphene Flagship Core 3 project (GA- 881603) as well as the Agence Nationale de la Recherche through the Labex project CSC (ANR-10- LABX-0026 CSC) within the Investissement d'Avenir program (ANR-10-120 IDEX-0002-02), the International Center for Frontier Research in Chemistry (icFRC) the Institut Universitaire de France (IUF), the Max Planck Society, as well as the German Research Foundation (DFG – Projektnummer 182087777 – SFB 951). The Gutenberg Research College of the Johannes Gutenberg University of Mainz is also acknowledged.

Received: ((will be filled in by the editorial staff))
Revised: ((will be filled in by the editorial staff))
Published online: ((will be filled in by the editorial staff))

References

[1] a) J. Cai, P. Ruffieux, R. Jaafar, M. Bieri, T. Braun, S. Blankenburg, M. Muoth, A. P. Seitsonen, M. Saleh, X. Feng, K. Müllen, R. Fasel, *Nature* **2010**, *466*, 470; b) S. Kawai, A. Benassi, E. Gnecco, H. Söde, R. Pawlak, X. Feng, K. Müllen, D. Passerone, C. A. Pignedoli, P. Ruffieux, R. Fasel, E. Meyer, *Science* **2016**, *351*, 957; c) J. Cai, C. A. Pignedoli, L. Talirz, P. Ruffieux, H. Söde, L. Liang, V. Meunier, R. Berger, R. Li, X. Feng, K. Müllen, R. Fasel, *Nat. Nanotechnol.* **2014**, *9*, 896; d) M. Koch, F. Ample, C. Joachim, L. Grill, *Nat. Nanotechnol.* **2012**, *7*, 713; e) G. Z. Magda, X. Jin, I. Hagymasi, P. Vancso, Z. Osvath, P. Nemes-Incze, C. Hwang, L. P. Biro, L. Tapaszto, *Nature* **2014**, *514*, 608; f) P. Ruffieux, S. Wang, B. Yang, C. Sánchez-Sánchez, J. Liu, T. Dienel, L. Talirz, P. Shinde, C. A. Pignedoli, D. Passerone, T. Dumslaff, X. Feng, K. Müllen, R. Fasel, *Nature* **2016**, *531*, 489; g) A. N. Sokolov, F. L. Yap, N. Liu, K. Kim, L. Ci, O. B. Johnson, H. Wang, M. Vosgueritchian, A. L. Koh, J. Chen, J. Park, Z. Bao, *Nat. Commun.* **2013**, *4*, 2402.

[2] L. Talirz, P. Ruffieux, R. Fasel, *Adv. Mater.* **2016**, *28*, 6222.

[3] a) A. Narita, X.-Y. Wang, X. Feng, K. Mullen, *Chem. Soc. Rev.* **2015**, *44*, 6616; b) N. Richter, Z. Chen, M.-L. Braatz, F. Musseau, N.-E. Weber, A. Narita, K. Müllen, M. Kläui, *Ann. Phys.* **2017**, *529*, 1700051; c) G. D. Nguyen, H.-Z. Tsai, A. A. Omrani, T. Marangoni, M. Wu, D. J. Rizzo, G. F. Rodgers, R. R. Cloke, R. A. Durr, Y. Sakai, F. Liou, A. S. Aikawa, J. R. Chelikowsky, S. G. Louie, F. R. Fischer, M. F. Crommie, *Nat. Nanotechnol.* **2017**, *12*, 1077; d) P. Pachfule, D. Shinde, M. Majumder, Q. Xu, *Nat. Chem.* **2016**, *8*, 718; e) X. Yu, B. Wang, D. Gong, Z. Xu, B. Lu, *Adv. Mater.* **2016**, *29*, 1604118; f) X. Li, X. Wang, L. Zhang, S. Lee, H. Dai, *Science* **2008**, *319*, 1229; g) C. Zhang, Z. Peng, J. Lin, Y. Zhu, G. Ruan, C.-C. Hwang, W. Lu, R. H. Hauge, J. M. Tour, *ACS Nano* **2013**, *7*, 5151.

[4] a) D. Qi, Z. Liu, Y. Liu, W. R. Leow, B. Zhu, H. Yang, J. Yu, W. Wang, H. Wang, S. Yin, X. Chen, *Adv. Mater.* **2015**, *27*, 5559; b) Z. Xiang, Q. Dai, J.-F. Chen, L. Dai, *Adv. Mater.* **2016**, *28*, 6253; c) W. Yuan, Y. Zhou, Y. Li, C. Li, H. Peng, J. Zhang, Z. Liu, L. Dai, G. Shi, *Sci. Rep.* **2013**, *3*, 2248.

[5] M. Y. Han, B. Özyilmaz, Y. Zhang, P. Kim, *Phys. Rev. Lett.* **2007**, *98*, 206805.

[6] a) D. V. Kosynkin, A. L. Higginbotham, A. Sinitskii, J. R. Lomeda, A. Dimiev, B. K. Price, J. M. Tour, *Nature* **2009**, *458*, 872; b) L. Jiao, X. Wang, G. Diankov, H. Wang, H. Dai, *Nat. Nanotechnol.* **2010**, *5*, 321.

[7] D. Gunlycke, D. A. Areshkin, C. T. White, *Appl. Phys. Lett.* **2007**, *90*, 142104.

[8] K. Müllen, *ACS Nano* **2014**, *8*, 6531.

[9] A. Narita, X. Feng, K. Müllen, *Chem. Rec.* **2015**, *15*, 295.

[10] A. Narita, X. Feng, Y. Hernandez, S. A. Jensen, M. Bonn, H. Yang, I. A. Verzhbitskiy, C. Casiraghi, M. R. Hansen, A. H. R. Koch, G. Fytas, O. Ivasenko, B. Li, K. S. Mali, T. Balandina, S. Mahesh, S. De Feyter, K. Müllen, *Nat. Chem.* **2014**, *6*, 126.

[11] Y. Huang, Y. Mai, U. Beser, J. Teyssandier, G. Velpula, H. van Gorp, L. A. Straasø, M. R. Hansen, D. Rizzo, C. Casiraghi, R. Yang, G. Zhang, D. Wu, F. Zhang, D. Yan, S. De Feyter, K. Müllen, X. Feng, *J. Am. Chem. Soc.* **2016**, *138*, 10136.

[12] a) M. Shekhirev, T. H. Vo, D. A. Kunkel, A. Lipatov, A. Enders, A. Sinitskii, *RSC Adv.* **2017**, *7*, 54491; b) A. N. Abbas, G. Liu, A. Narita, M. Orosco, X. Feng, K. Müllen, C. Zhou, *J. Am. Chem. Soc.* **2014**; c) T. H. Vo, M. Shekhirev, D. A. Kunkel, M. D. Morton, E. Berglund, L. Kong, P. M. Wilson, P. A. Dowben, A. Enders, A. Sinitskii, *Nat. Commun.* **2014**, *5*, 3189; d) U. Zschieschang, H. Klauk, I. B. Müeller, A. J. Strudwick, T. Hintermann, M. G. Schwab, A. Narita, X. Feng, K. Müellen, R. T. Weitz, *Adv. Electron. Mater.* **2015**, *1*, 1400010; e) M. Shekhirev, T. H. Vo, M. Mehdi Pour, A. Lipatov, S. Munukutla, J. W. Lyding, A. Sinitskii, *ACS Appl. Mater. Interfaces* **2017**, *9*, 693; f) P. Fantuzzi, L. Martini, A. Candini, V. Corradini, U. del Pennino, Y. Hu, X. Feng, K. Müllen, A. Narita, M. Affronte, *Carbon* **2016**, *104*, 112; g) A. Radocea, T. Sun, T. H. Vo, A. Sinitskii, N. R. Aluru, J. W.

Lyding, *Nano Lett.* **2017**, *17*, 170; h) S. Zhao, L. Rondin, G. Delport, C. Voisin, U. Beser, Y. Hu, X. Feng, K. Müllen, A. Narita, S. Campidelli, J. S. Lauret, *Carbon* **2017**, *119*, 235.
[13] K. R. Paton, E. Varrla, C. Backes, R. J. Smith, U. Khan, A. O'Neill, C. Boland, M. Lotya, O. M. Istrate, P. King, T. Higgins, S. Barwich, P. May, P. Puczkarski, I. Ahmed, M. Moebius, H. Pettersson, E. Long, J. Coelho, S. E. O'Brien, E. K. McGuire, B. M. Sanchez, G. S. Duesberg, N. McEvoy, T. J. Pennycook, C. Downing, A. Crossley, V. Nicolosi, J. N. Coleman, *Nat. Mater.* **2014**, *13*, 624.
[14] a) Y. Hernandez, V. Nicolosi, M. Lotya, F. M. Blighe, Z. Sun, S. De, I. T. McGovern, B. Holland, M. Byrne, Y. K. Gun'Ko, J. J. Boland, P. Niraj, G. Duesberg, S. Krishnamurthy, R. Goodhue, J. Hutchison, V. Scardaci, A. C. Ferrari, J. N. Coleman, *Nat. Nanotechnol.* **2008**, *3*, 563; b) A. Ciesielski, P. Samorì, *Chem. Soc. Rev.* **2014**, *43*, 381.
[15] J. M. Hughes, Y. Hernandez, D. Aherne, L. Doessel, K. Müllen, B. Moreton, T. W. White, C. Partridge, G. Costantini, A. Shmeliov, M. Shannon, V. Nicolosi, J. N. Coleman, *J. Am. Chem. Soc.* **2012**, *134*, 12168.
[16] G. Soavi, S. Dal Conte, C. Manzoni, D. Viola, A. Narita, Y. Hu, X. Feng, U. Hohenester, E. Molinari, D. Prezzi, K. Müllen, G. Cerullo, *Nat. Commun.* **2016**, *7*, 11010.
[17] a) I. A. Verzhbitskiy, M. D. Corato, A. Ruini, E. Molinari, A. Narita, Y. Hu, M. G. Schwab, M. Bruna, D. Yoon, S. Milana, X. Feng, K. Müllen, A. C. Ferrari, C. Casiraghi, D. Prezzi, *Nano Lett.* **2016**, *16*, 3442; b) D. Rizzo, D. Prezzi, A. Ruini, V. Nagyte, A. Keerthi, A. Narita, U. Beser, F. Xu, Y. Mai, X. Feng, K. Müllen, E. Molinari, C. Casiraghi, *Phys. Rev. B* **2019**, *100*, 045406.
[18] a) A. Ciesielski, S. Haar, M. El Gemayel, H. Yang, J. Clough, G. Melinte, M. Gobbi, E. Orgiu, M. V. Nardi, G. Ligorio, V. Palermo, N. Koch, O. Ersen, C. Casiraghi, P. Samorì, *Angew. Chem. Int. Ed.* **2014**, *53*, 10355; b) S. Haar, A. Ciesielski, J. Clough, H. Yang, R. Mazzaro, F. Richard, S. Conti, N. Merstorf, M. Cecchini, V. Morandi, C. Casiraghi, P. Samorì, *Small* **2015**, *11*, 1691.
[19] C. E. P. Villegas, P. B. Mendonça, A. R. Rocha, *Sci. Rep.* **2014**, *4*, 6579.
[20] Y.-Z. Tan, B. Yang, K. Parvez, A. Narita, S. Osella, D. Beljonne, X. Feng, K. Müllen, *Nat. Commun.* **2013**, *4*, 2646.
[21] P. Samorí, N. Severin, C. D. Simpson, K. Müllen, J. P. Rabe, *J. Am. Chem. Soc.* **2002**, *124*, 9454.
[22] a) R. Ulbricht, E. Hendry, J. Shan, T. F. Heinz, M. Bonn, *Rev. Mod. Phys* **2011**, *83*, 543; b) I. Ivanov, Y. Hu, S. Osella, U. Beser, H. I. Wang, D. Beljonne, A. Narita, K. Müllen, D. Turchinovich, M. Bonn, *J. Am. Chem. Soc.* **2017**, *139*, 7982; c) W. Niu, J. Ma, P. Soltani, W. Zheng, F. Liu, A. A. Popov, J. J. Weigand, H. Komber, E. Poliani, C. Casiraghi, J. Droste, M. R. Hansen, S. Osella, D. Beljonne, M. Bonn, H. I. Wang, X. Feng, J. Liu, Y. Mai, *J. Am. Chem. Soc.* **2020**, *142*, 18293; d) W. Zheng, M. Bonn, H. I. Wang, *Nano Lett.* **2020**, *20*, 5807; e) X. Yao, W. Zheng, S. Osella, Z. Qiu, S. Fu, D. Schollmeyer, B. Müller, D. Beljonne, M. Bonn, H. I. Wang, K. Müllen, A. Narita, *J. Am. Chem. Soc.* **2021**, *143*, 5654.
[23] a) A. Tries, S. Osella, P. Zhang, F. Xu, C. Ramanan, M. Kläui, Y. Mai, D. Beljonne, H. I. Wang, *Nano Lett.* **2020**, *20*, 2993; b) F. Xu, C. Yu, A. Tries, H. Zhang, M. Kläui, K. Basse, M. R. Hansen, N. Bilbao, M. Bonn, H. I. Wang, Y. Mai, *J. Am. Chem. Soc.* **2019**, *141*, 10972.
[24] Z. Liu, Z. Chen, C. Wang, H. I. Wang, M. Wuttke, X.-Y. Wang, M. Bonn, L. Chi, A. Narita, K. Müllen, *J. Am. Chem. Soc.* **2020**, *142*, 17881.
[25] Z. Liu, H. Zhang, M. Eredia, H. Qiu, W. Baaziz, O. Ersen, A. Ciesielski, M. Bonn, H. I. Wang, P. Samorì, *ACS Nano* **2019**, *13*, 9431.
[26] Z. S. Wu, K. Parvez, X. Feng, K. Müllen, *Nat. Commun.* **2013**, *4*, 2487.
[27] a) M. F. El-Kady, R. B. Kaner, *Nat. Commun.* **2013**, *4*, 1475; b) W. Gao, N. Singh, L. Song, Z. Liu, A. L. M. Reddy, L. Ci, R. Vajtai, Q. Zhang, B. Wei, P. M. Ajayan, *Nat.*

Nanotechnol. **2011**, *6*, 496; c) A. Ghosh, V. T. Le, J. J. Bae, Y. H. Lee, *Sci. Rep.* **2013**, *3*, 2939.
[28] Z. Niu, L. Zhang, L. Liu, B. Zhu, H. Dong, X. Chen, *Adv. Mater.* **2013**, *25*, 4035.
[29] Y. Tao, X. Xie, W. Lv, D.-M. Tang, D. Kong, Z. Huang, H. Nishihara, T. Ishii, B. Li, D. Golberg, F. Kang, T. Kyotani, Q.-H. Yang, *Sci. Rep.* **2013**, *3*, 2975.
[30] a) J. Chmiola, C. Largeot, P.-L. Taberna, P. Simon, Y. Gogotsi, *Science* **2010**, *328*, 480; b) P. Huang, C. Lethien, S. Pinaud, K. Brousse, R. Laloo, V. Turq, M. Respaud, A. Demortière, B. Daffos, P. L. Taberna, B. Chaudret, Y. Gogotsi, P. Simon, *Science* **2016**, *351*, 691.
[31] T. Lin, I.-W. Chen, F. Liu, C. Yang, H. Bi, F. Xu, F. Huang, *Science* **2015**, *350*, 1508.
[32] Z.-S. Wu, Y.-Z. Tan, S. Zheng, S. Wang, K. Parvez, J. Qin, X. Shi, C. Sun, X. Bao, X. Feng, K. Müllen, *J. Am. Chem. Soc.* **2017**, *139*, 4506.
[33] D. Pech, M. Brunet, H. Durou, P. Huang, V. Mochalin, Y. Gogotsi, P.-L. Taberna, P. Simon, *Nat. Nanotechnol.* **2010**, *5*, 651.

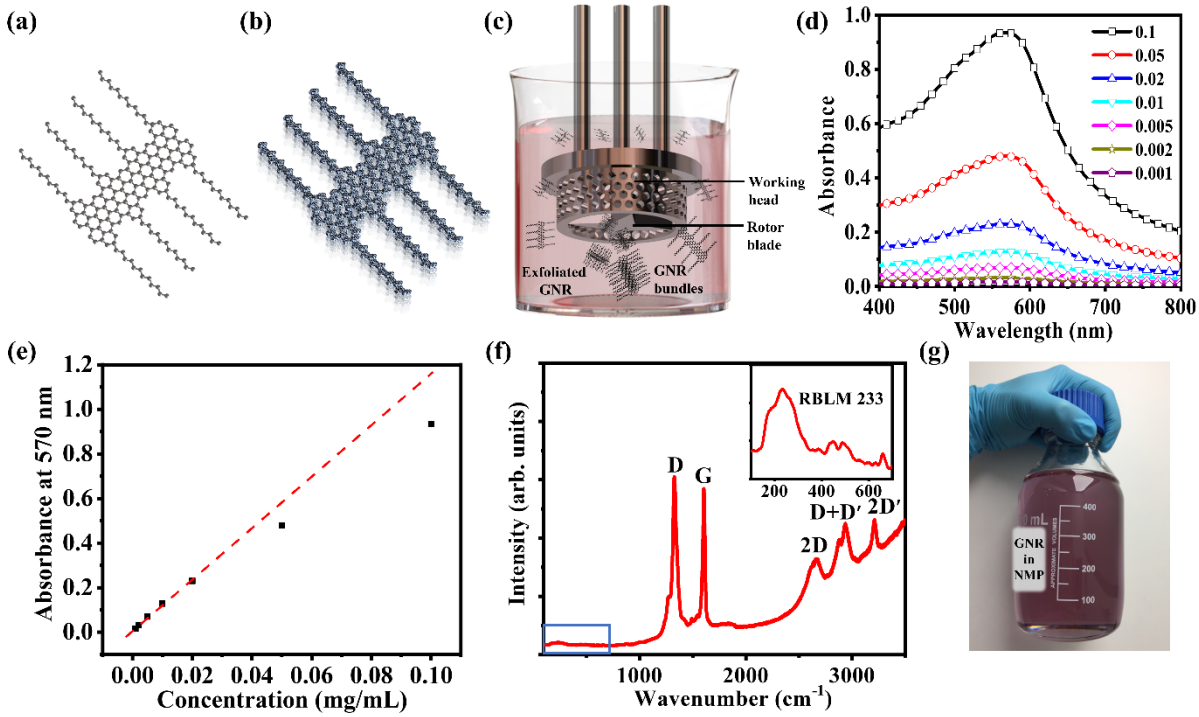

Figure 1. a) Molecular model of 4-CGNR. b) Schematic illustration of the bundles based on the aggregation of 4-CGNR. c) Schematic illustration of the exfoliation process of 4-CGNR bundles by shear-mixing method. d) UV-Vis absorption of 4-CGNR dispersion with different concentrations, from 0.001 to 0.1 mg mL^{-1}. e) Plot of absorbance at 570 nm as a function of 4-CGNR concentration, which shows a good linear fitting with R^2=0.996 at lower concentrations. f) Raman spectra of 4-CGNR film. Inset shows a magnified area of the spectra (100-700 cm^{-1}) to display the characteristic RBLM peak at 233 cm^{-1}. g) Image of well exfoliated 4-CGNR dispersion in NMP, demonstrating the potential scale-up production of GNRs.

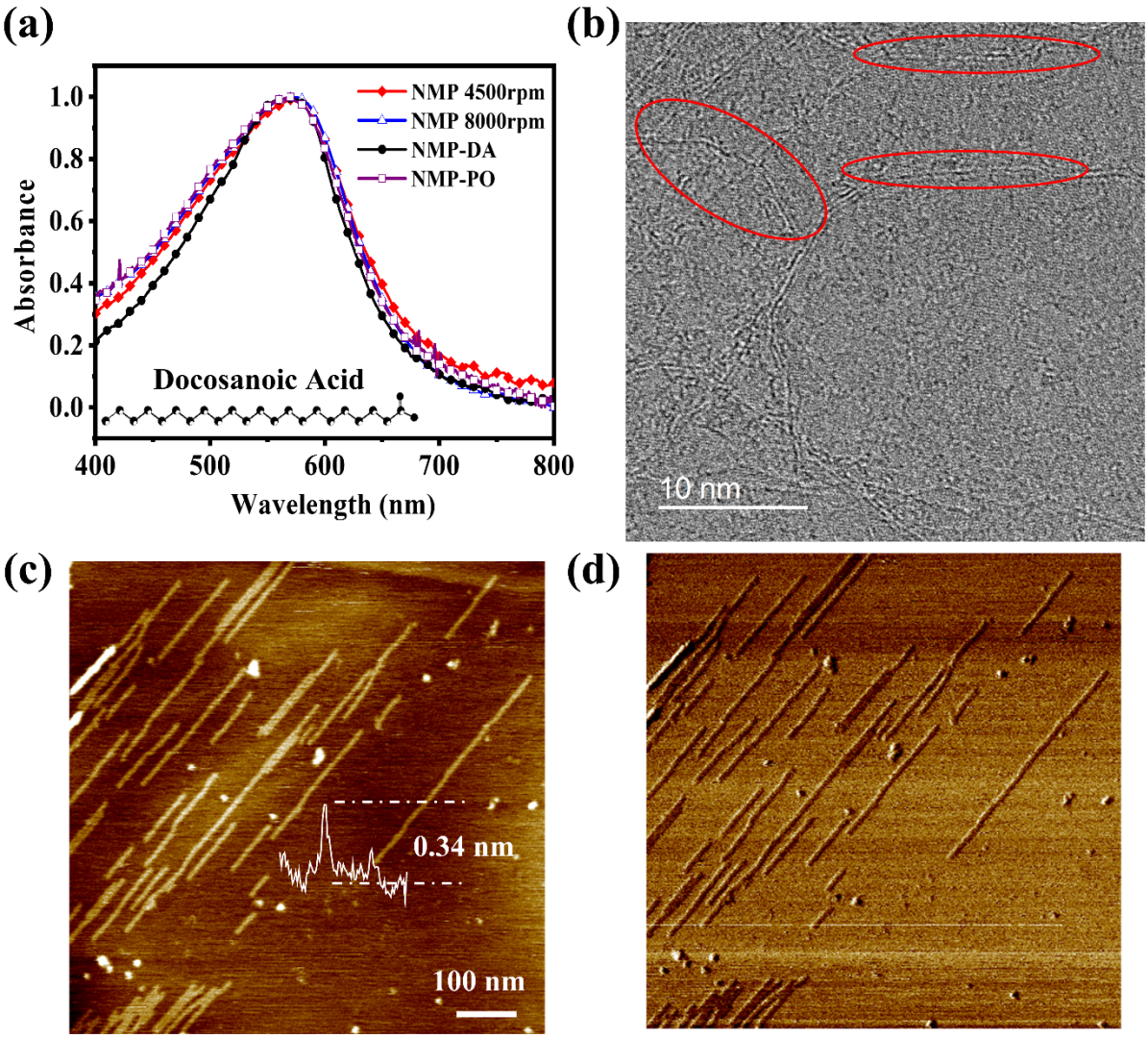

Figure 2. a) UV-Vis absorption of 4-CGNR dispersion in NMP with different rotor speeds of 4500 and 8000 rpm, and different molecular interactions with docosanoic acid (DA) and 1-Phenyloctane (PO). b) HR-TEM image of 4-CGNR. c, d) AFM height and phase image of 4-CGNR on HOPG.

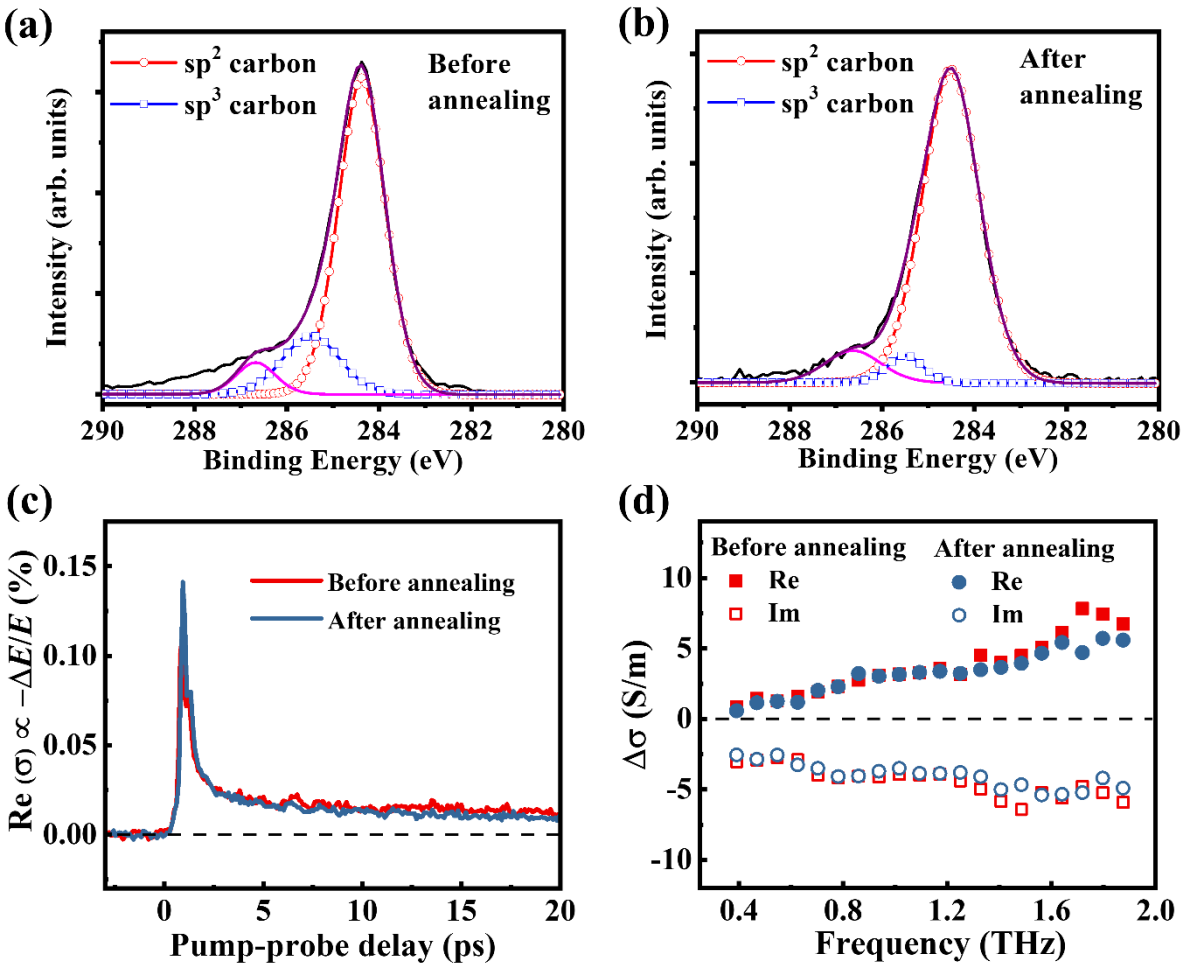

Figure 3. High-resolution XPS of the C 1s spectrum of 4-CGNR film a) before and b) after annealing. c) Time-resolved terahertz photoconductivity (proportional to the relative changes in the transmitted field, −ΔE/E) of 4-CGNR films before and after annealing treatment. The samples are photoexcited by a 3.1 eV-energy laser pulse with a photon density of 3.8×10^{14} cm^{-2}. d) Frequency-resolved terahertz conductivity of 4-CGNR films before and after annealing treatment measured at ~1.4 ps after photoexcitation. The red and blue symbols represent the real and imaginary conductivity, respectively. The solid lines are fits to the Drude-Smith model.

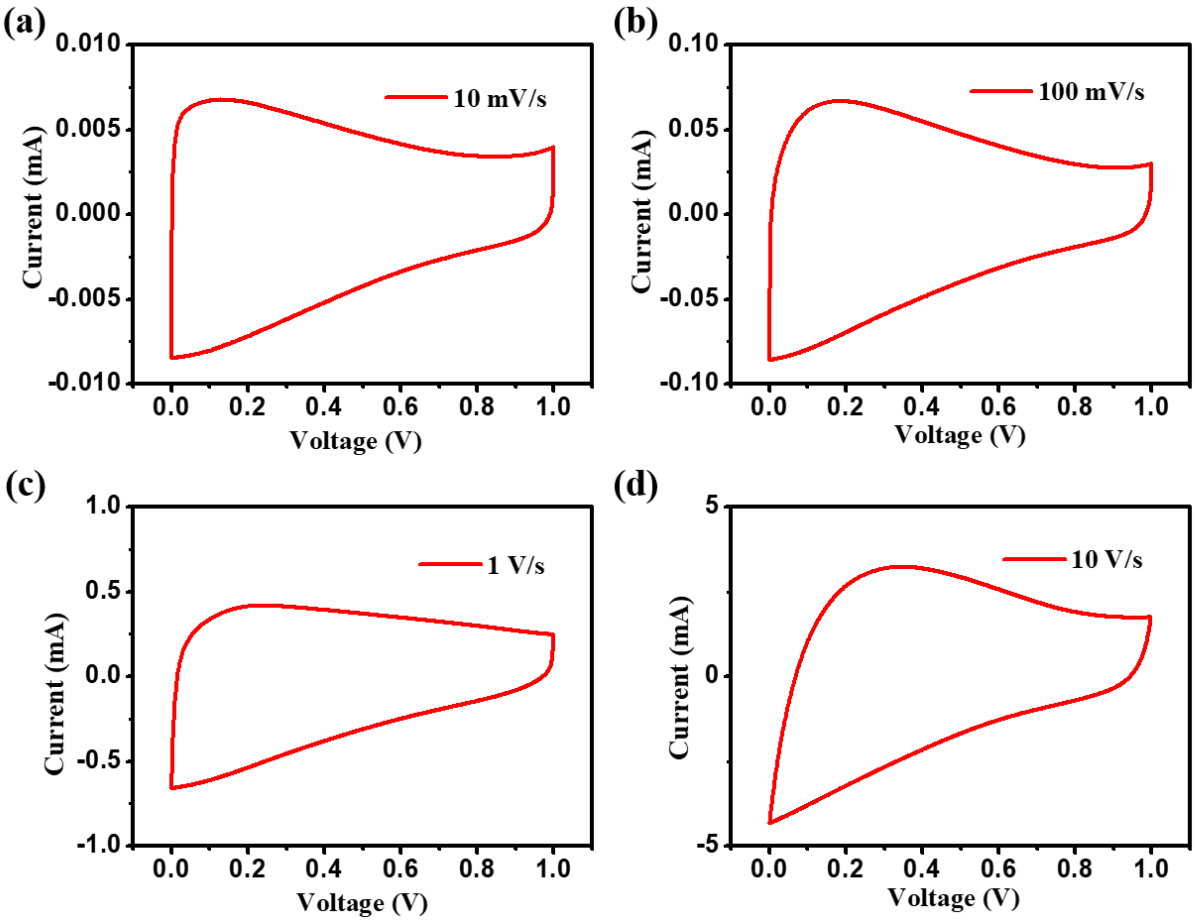

Figure 4. CV curves of micro-supercapacitor based on shear-mix exfoliated 4-CGNR film, performed at different scan rates ranging from 10 to 10000 mV s^{-1}, with a potential window from 0 to 1 V.

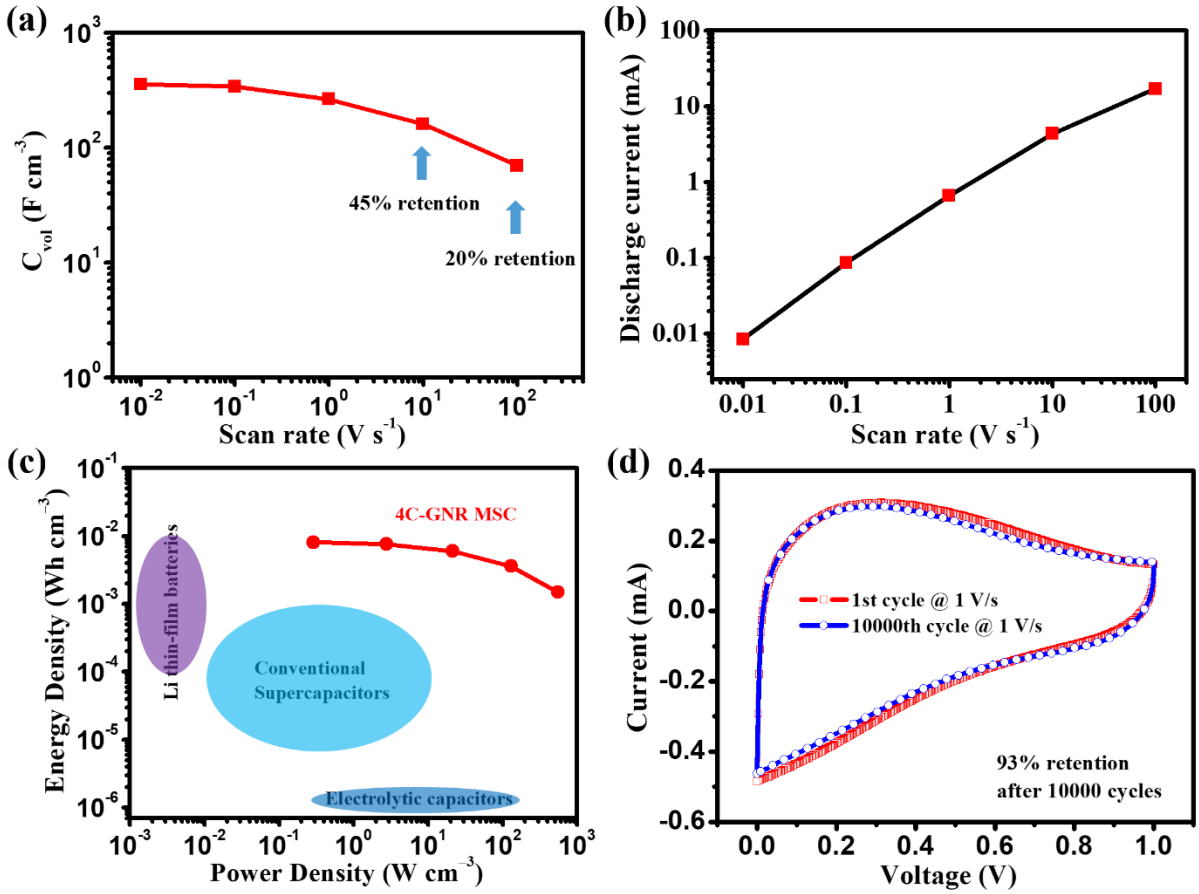

Figure 5. a) Evolution of the volumetric capacitance versus scan rate based on 4-CGNR film. b) Discharge current of 4-CGNR based MSC as a function of scan rate. c) Ragone plot of commercially available Li thin-film battery and electrolytic capacitor compared with 4-CGNR based MSC. d) Stability test: CV curves of the 1st and 10000th cycle of 4-CGNR based MSC, showing a capacitance retention of over 93% at a high operating speed of 1 V s^{-1}.